Atmos. Chem. Phys., 14, 831–846, 2014
www.atmos-chem-phys.net/14/831/2014/
doi:10.5194/acp-14-831-2014

Atmospheric Chemistry and Physics
Open Access

Stratospheric ozone trends and variability as seen by SCIAMACHY from 2002 to 2012

C. Gebhardt[1], A. Rozanov[1], R. Hommel[1], M. Weber[1], H. Bovensmann[1], J. P. Burrows[1], D. Degenstein[2], L. Froidevaux[3], and A. M. Thompson[4]

[1]Institute of Environmental Physics (IUP), University of Bremen, Bremen, Germany
[2]University of Saskatchewan, Saskatoon, Canada
[3]Jet Propulsion Laboratory, California Institute of Technology, Pasadena, CA, USA
[4]NASA/Goddard Space Flight Center, Greenbelt, MD, USA

Correspondence to: C. Gebhardt (gebhardt@iup.physik.uni-bremen.de)

Received: 20 March 2013 – Published in Atmos. Chem. Phys. Discuss.: 26 April 2013
Revised: 5 November 2013 – Accepted: 12 December 2013 – Published: 24 January 2014

Abstract. Vertical profiles of the rate of linear change (trend) in the altitude range 15–50 km are determined from decadal O_3 time series obtained from SCIAMACHY[1]/ENVISAT[2] measurements in limb-viewing geometry. The trends are calculated by using a multivariate linear regression. Seasonal variations, the quasi-biennial oscillation, signatures of the solar cycle and the El Niño–Southern Oscillation are accounted for in the regression. The time range of trend calculation is August 2002–April 2012. A focus for analysis are the zonal bands of 20° N–20° S (tropics), 60–50° N, and 50–60° S (midlatitudes). In the tropics, positive trends of up to 5 % per decade between 20 and 30 km and negative trends of up to 10 % per decade between 30 and 38 km are identified. Positive O_3 trends of around 5 % per decade are found in the upper stratosphere in the tropics and at midlatitudes. Comparisons between SCIAMACHY and EOS MLS[3] show reasonable agreement both in the tropics and at midlatitudes for most altitudes. In the tropics, measurements from OSIRIS[4]/Odin and SHADOZ[5] are also analysed. These yield rates of linear change of O_3 similar to those from SCIAMACHY. However, the trends from SCIAMACHY near 34 km in the tropics are larger than MLS and OSIRIS by a factor of around two.

1 Introduction

The stratospheric O_3 layer shields the Earth from UVB and UVC radiation in the 240–320 nm range. The absorbed energy is the main heat source of the stratosphere, and also drives the atmospheric circulation in the upper atmosphere (e.g. Weber et al., 2011). The abundance of stratospheric O_3 is sensitive to both chemical and dynamical factors and has been altered by anthropogenic activity. The most prominent example of human impact on the O_3 layer is the Antarctic O_3 hole, which is caused by anthropogenically released chlorine and bromine compounds. In order to protect the O_3 layer, the production of halogenated source gases was banned by the Montreal Protocol of 1987 and its amendments. A slowdown of the O_3 decline and even an onset of a recovery have been inferred from observations (Newchurch et al., 2003; Yang et al., 2006; WMO, 2007). The recovery of the global stratospheric O_3 layer to values observed before the chlorofluorocarbon (CFC)-driven depletion is, however, not expected before the middle of this century (WMO, 2011).

Measurements of O_3 have a long tradition, and various trend studies have been performed using data from the last few decades (WMO, 2007). In recent years, several trend studies have investigated the impacts of O_3-depleting substances (ODS) and dynamical forcings affecting the O_3

[1]SCanning Imaging Absorption spectroMeter for Atmospheric CHartographY
[2]European environmental research satellite
[3]Earth Observing System (EOS) Microwave Limb Sounder (MLS)
[4]Optical Spectrograph and InfraRed Imager System
[5]Southern Hemisphere ADditional OZonesondes

shield (WMO, 2007, 2011). The majority of these trend assessments agreed that the present stage of stratospheric O_3 is somewhere between the rate of depletion slowing down and a subsequent turnaround phase, expected as a result of the measures implemented within the Montreal Protocol and its amendments. This manuscript contributes to our knowledge of stratospheric O_3 and its changes during the period following the turnaround in stratospheric halogens in the late 1990s, where the halogen load, still high, is slowly declining.

Vertically resolved O_3 trends have been derived from observations by satellite instruments, ground-based lidars and microwave radiometers, and balloon-borne ozonesondes (Steinbrecht et al., 2006; Jones et al., 2009; Randel and Thompson, 2011; Mieruch et al., 2012). In Mieruch et al. (2012), O_3 trends from SCIAMACHY and those inferred from a range of instruments were compared within the time from 2002 to 2008 with the main focus on possible instrumental and algorithmic issues. Analysing a number of different satellite datasets, Jones et al. (2009) inferred O_3 trends from a multi-instrument mean between 1979 and 2008. SCIAMACHY, OSIRIS/Odin, and SMR/Odin contributed data starting in the years 2002 and 2001 respectively. Jones et al. (2009) showed that these satellite data agreed with each other to a high extent. After 1997, Jones et al. (2009) identified positive midlatitude O_3 trends between 35 and 45 km on the order of a few percent per decade. These findings are corroborated by Steinbrecht et al. (2006, 2009) by using ground-based measurements. As the upper stratosphere is highly sensitive to halogen chemistry (WMO, 1999), these results may be interpreted as signs of the onset of a turnaround in the O_3 abundance in response to declining halogens. Analysing a merged dataset from satellites and ozonesondes, Randel and Thompson (2011) identified negative O_3 trends in the lowermost tropical stratosphere. These were primarily attributed to dynamical factors, namely enhanced tropical upwelling.

In this study, a global O_3 dataset obtained from the SCIAMACHY instrument on-board ENVISAT is investigated. SCIAMACHY was in routine operation from August 2002 until ENVISAT suddenly and unexpectedly failed on 8 April 2012. In its limb-viewing geometry, SCIAMACHY performed measurements of the scattered solar radiation. These limb measurements are used to retrieve vertical profiles of trace gases and aerosols and to detect clouds.

Rates of linear change or trends in the SCIAMACHY limb O_3 time series are determined in our investigation for the time range from August 2002 to April 2012. These trends are presented as functions of altitude and latitude. The resulting vertical trend profiles of O_3 are presented for latitudes between 60° N and 60° S. The trends from SCIAMACHY are compared with those derived from OSIRIS/Odin and SHADOZ ozonesondes in the tropics and with those from EOS MLS in the tropics and at midlatitudes.

This paper is structured as follows. Section 2 describes briefly the SCIAMACHY limb O_3 retrieval. The multivariate linear regression, used in our study, is introduced and explained in Sect. 3. The O_3 time series from SCIAMACHY and their regression models are described in Sect. 4. In Sect. 5, the vertical profiles of the rate of linear change or trend of the O_3 retrieved from SCIAMACHY measurements are presented. O_3 trend profiles from SCIAMACHY are compared with those from EOS MLS and OSIRIS/Odin, other atmospheric limb sounders, in Sect. 6. In addition, comparisons are performed in the inner tropics including SHADOZ ozonesondes. Section 7 discusses atmospheric phenomena potentially responsible for the observed O_3 trends. In Sect. 8, sources of errors are discussed. Section 9 summarises the main results obtained in this study.

2 SCIAMACHY limb ozone

The European environmental research satellite ENVISAT hosted ten instruments, which were operational until the sudden loss of contact with ENVISAT on 8 April 2012. SCIAMACHY observed electromagnetic radiation upwelling from the Earth's atmosphere in 3 measurement modes: occultation, nadir, and limb geometry. Detailed information on the instrument and mission objectives is provided by Burrows et al. (1995) and Bovensmann et al. (1999). In limb-viewing geometry, the instrument scanned the horizon in 3.3 km steps from −3 to 92 km (0 to 92 km since October 2010). This vertical sampling and the instantaneous field of view (∼ 2.6 km in vertical direction at the tangent point) defined the vertical resolution, which was typically 3–4 km. ENVISAT was in a Sun-synchronous orbit with an inclination of 98°. This resulted in global coverage for SCIAMACHY limb measurements being achieved within 6 days at the Equator and less elsewhere.

The SCIAMACHY results presented here use the limb O_3 retrieval version 2.9 of IUP Bremen. As an intermediate retrieval result, monthly mean O_3 data are gridded horizontally into 5° latitude × 15° longitude and vertically into 1 km altitude. The overall altitude range of O_3 retrieval is 10 to 75 km. As the satellite retrieval often suffered from cloud interference below 15 km, only altitudes above 15 km are used in this study.

Comparing SCIAMACHY limb O_3 data to vertically resolved O_3 datasets from other instruments, Mieruch et al. (2012) showed that comparison results are not significantly changed using either collocated measurement pairs or zonal monthly means of gridded data. This highlights that zonal monthly means are appropriate for performing instrument comparisons. Our investigation uses zonal mean O_3 data for the latitudes defined by the gridding of data as well as for wider latitude bands. Determining the rate of linear change or trend for all altitudes between 15 and 50 km results in vertical profiles of O_3 trends.

The zonal monthly mean values are calculated as arithmetic means because the errors of single measurements are

expected to be normally distributed and no issue with outliers is known. Any of these zonal monthly means is typically composed of several hundreds of single measurements. Hence, the random errors of zonal monthly means can be deemed as negligible. Trend uncertainties used in the following are calculated from the covariance matrix of regression.

The boundaries of 60° N and 60° S are chosen for this investigation to avoid any effects which are directly related to the polar vortex and because of gaps in the SCIAMACHY sampling during the high-latitude winter. In order to avoid possible influences of the South Atlantic Anomaly, measurements with tangent point coordinates between longitudes of 90° W and 0° W and latitudes south of 20° S are excluded from this analysis (it is worth noting that a typical difference in latitude between instrument and tangent point coordinates of around 20° is taken into account by the criteria used).

3 Trend determination

3.1 Multivariate linear regression

A multivariate linear regression is applied to the datasets with the autocorrelation of consecutive values accounted for by the Cochrane–Orcutt transformation (Cochrane and Orcutt, 1949). The observed values of autocorrelation are similar to those shown in Mieruch et al. (2012). The regression is unweighted. The following terms are used in the regression:

$$\mu + \omega t + \sum_{j=1}^{4} \left(\beta_{1j} \sin(\frac{2\pi j t}{12}) + \beta_{2j} \cos(\frac{2\pi j t}{12}) \right) + R(t), \quad (1)$$

where t is the time in months and μ, ω, and β_{11}, β_{12}, …, β_{23}, β_{24} are the fitting parameters. The harmonics with 12-, 6-, 4-, and 3-month periods, $j = 1, 2, 3, 4$, a sine and cosine term each, are used to represent seasonal changes. The harmonics of 12 and 6 months approximate the annual and semi-annual cycles. The combination of sine and cosine terms provides a flexible adjustment to any phase of the (semi-)annual variation. As discussed by Stiller et al. (2012), the terms having 4- and 3-month periods improve the fit quality because the oscillation patterns are possibly compressed or stretched with respect to a harmonic shape. In addition, a linear fit having a gradient or slope ω and an intercept μ is included in the regression analysis. The gradient represents the O_3 trend at a given altitude. The 1σ value defined by the covariance matrix of regression coefficients serves as trend uncertainty. It is also used to draw error bars of trends in subsequent figures. The trends and their uncertainties are presented in relative units of % dec^{-1}, i.e. percent per decade (relative with respect to the mean value of the underlying time series). The criterion for the trend being significant at the 95 % confidence level is that the absolute ratio of the trend to its uncertainty is larger than 2 (Tiao et al., 1990). As discussed later in Sect. 3.2, it is also advantageous to extend the linear regression (see Eq. 1) by additional terms representing the quasi-biennial oscillation (QBO), the solar cycle (SC), and the El Niño–Southern Oscillation (ENSO):

$$R(t) = \mathrm{QBO}(t) + \mathrm{SC}(t) + \mathrm{ENSO}(t). \quad (2)$$

At northern midlatitudes, Eq. (1) is optimised because of the strong interannual variability of the annual cycle of O_3. In the 15–26 km range of the 60–50° N latitude band, the cumulative eddy heat flux (based on ERA-Interim, 50 hPa eddy heat flux integrated from 45° N to 75° N, cumulation starts in October) is fitted instead of harmonic terms. The cumulative eddy heat flux is a proxy accounting for the wave-driven O_3 accumulation in winter and early spring. For 60–50° N, the interannual variability in total O_3 is found to be well approximated by the cumulative eddy heat flux (Dhomse et al., 2006). Here, correlation tests show that throughout the altitude range of 15–26 km, the proxy being time lagged by 2 months is optimum.

3.2 QBO, solar cycle, and ENSO signatures in ozone

The quasi-biennial oscillation (QBO) is a quasi-periodic signal observed in the tropical stratospheric zonal wind speed. It alternates between east and west phase with the period varying between 2 and 3 yr. Previous studies report a maximum QBO response of tropical O_3 in the altitude ranges of 20–27 km and 30–38 km (Zawodny and McCormick, 1991; Chipperfield et al., 1994).

In the tropics, the QBO response of O_3 is driven by effects related to the vertical transport (Butchart et al., 2003). The QBO-induced meridional circulation modulates the upwelling branch of the Brewer–Dobson circulation, leading to the largest changes of the O_3 volume mixing ratio (VMR) in the altitude range of large vertical gradients of the O_3 VMR, which are located below and above the maximum in the vertical O_3 VMR profiles. The result is a compacting (vertical squeezing) of the mean vertical O_3 VMR profile at westerly QBO phase and a lofting (vertical stretching) at easterly QBO phase. Around the maximum of the mean vertical profile of the O_3 VMR, where the vertical gradient changes sign, the phase change of the QBO response of O_3 takes place (Butchart et al., 2003). With the QBO phases modulating the Brewer–Dobson circulation, a QBO response is expected to be observed also in extratropical O_3 (Baldwin et al., 2001).

In the following, the 10 hPa and 30 hPa Singapore winds (Naujokat, 1986, available from http://www.geo.fu-berlin.de/en/met/ag/strat/produkte/qbo/) are used as fit proxies:

$$\mathrm{QBO}(t) = a\mathrm{QBO}_{10}(t) + b\mathrm{QBO}_{30}(t), \quad (3)$$

with a and b being their fit coefficients. The indices "10" and "30" denote the pressure level of the proxy. This approach is applied both in the tropics and extratropics to account for

any QBO effects. The monthly time series of the Singapore winds are smoothed by a 4-month running average before being used as QBO proxy. The same procedure is done with the Mg II index when used as a solar cycle proxy. Both proxies are not detrended.

The 11 yr solar cycle, which leads to pronounced variations of the solar radiation in the UV spectral range, is known to influence stratospheric O_3 (Gray et al., 2010). It is widely accepted that the solar cycle response of O_3 occurs without any time lag and at positive correlation (e.g. Soukharev and Hood, 2006; Remsberg and Lingenfelser, 2010). The solar cycle response of O_3 may extend from the tropics into the midlatitudes (SPARC CCMVal, 2010). In the following, the solar cycle proxy is included in the multivariate linear regression for any latitude analysed. A multi-instrument monthly average Mg II index – which is mainly based on GOME, SCIAMACHY, and GOME-2 observations over the time span under study – serves as solar cycle proxy. The underlying data can be obtained from http://www.iup.uni-bremen.de/gome/solar/MgII_composite.dat (Snow et al., 2013; Weber et al., 2013).

In addition to the QBO and the solar cycle, the O_3 time series may also be influenced by the El Niño Southern Oscillation (ENSO) (Randel et al., 2009; Randel and Thompson, 2011). Employing an ENSO proxy based on the Niño 3.4 index, Oman et al. (2013) previously demonstrated its applicability to reveal ENSO signatures in vertically resolved O_3 time series from EOS MLS. With the ENSO response of O_3 propagating towards higher altitudes, time lags between ENSO signatures in O_3 and ENSO proxies may arise. For instance, Randel et al. (2009) and Randel and Thompson (2011) employed ENSO proxies at a time lag of 2 months.

Similar to Oman et al. (2013), an ENSO proxy based on anomalies of the Niño 3.4 index (available from http://www.cpc.ncep.noaa.gov/data/indices/) is used in our study. Time lags are accounted for by the combined fit of the proxy and its time derivative:

$$\mathrm{ENSO}(t) = c\left[N_{34}(t) + \frac{\mathrm{d}N_{34}(t)}{\mathrm{d}t}\Delta(t)\right], \quad (4)$$

where N_{34} denotes the proxy and $\Delta(t)$ the time lag. Accounting for the non-linearity of $\frac{\mathrm{d}N_{34}(t)}{\mathrm{d}t}$, the fit is repeated with the lagged proxy until the remaining time lag approaches zero. This iteration starts at a time lag of 2 months. The time lag of the proxy not settling at a certain value (including zero) or becoming unrealistic is the criterion for omitting ENSO terms at regression. In practice, the latter is the case at extratropical latitudes and in the tropics at altitudes above 25 km. In the following, ENSO is considered at regression only at tropical latitudes (any latitude band within 20° N–20° S) in the 15–25 km altitude range. If the criterion for omitting ENSO terms is still fulfilled, the underlying time series is excluded from analysis (resulting in the gaps in the vertical trend profiles shown Figs. 8 and 11 and in the QBO amplitude/solar cycle response shown in Figs. A1 and A2).

4 Time series of ozone

Figures 1–6 show O_3 time series at the altitudes of 21 km, 35 km, and 44 km at northern midlatitudes (60–50° N) and in the tropics (20° N–20° S). The time series are overlaid by their fitting curves from the regression model, and the fit residuals are plotted below. The individual terms from the regression – i.e. the harmonic, QBO, solar cycle, and linear terms – are shown in corresponding panels below (in the tropics at 21 km, ENSO terms are included as well while, at northern midlatitudes at 21 km, eddy heat flux terms are shown instead of harmonic terms). The harmonic terms are shown comprising all periods used, i.e. 12, 6, 4, and 3 months, and also as combination of the terms with 4- and 3-month periods only. With the exception of 44 km at 60–50° N, the latter terms of 4- and 3-month periods improve the closure between time series and fitting curve, but do not change the amplitude of the harmonic terms substantially. The harmonic terms are overlaid by the time series with all fit terms with the exception of the harmonics subtracted. Any other component of the fitting curve is overlaid by the time series with all other fit terms removed accordingly.

At all altitudes, good fit quality is obtained. The use of harmonics for approximating the (semi-)annual oscillation as well as the combination of the 10 hPa and 30 hPa Singapore winds to fit QBO appears to be a sufficiently complete approach. The fit residuals are well within ±5 % to ±10 % of the fitted time series both at midlatitudes and in the tropics.

At 21 and 35 km at midlatitudes, the annual cycle terms (green curve has an annual pattern) dominate in the fitting curve. At 21 km, O_3 has its annual maximum in late winter/early spring and declines throughout summer. At 35 km, the annual maximum of O_3 is reached in late spring/early summer, persisting for the summer months. At 44 km at midlatitudes, the harmonic terms have two maxima and minima per year. The annual minimum occurs in summer and a secondary minimum in winter. These patterns are explained as follows: at 21 km, the periodic variability of O_3 is dominated by transport effects in winter, leading to an accumulation of O_3, and by catalytic O_3 depletion in summer which is responsible for the descending branch of the annual cycle. At 35 km and 44 km, the periodic variability is governed by photochemical O_3 production and by catalytic O_3 depletion respectively, both being at its maximum in summer (Perliski et al., 1989). At 35 km, the annual maximum in summer driven by photochemical production is flattened by catalytic depletion which is of minor consequence. At 44 km, catalytic depletion has gained control leading to the annual minimum in summer. Overlaid photochemical production of O_3 leads to a secondary minimum in winter.

At 21 km in the tropics, the annual cycle and the QBO make comparable contributions to the fitting curve. Discernible contributions are also made by the ENSO. The annual cycle has its maximum in the Northern Hemisphere summer. It resembles well the phase of the annual oscillation

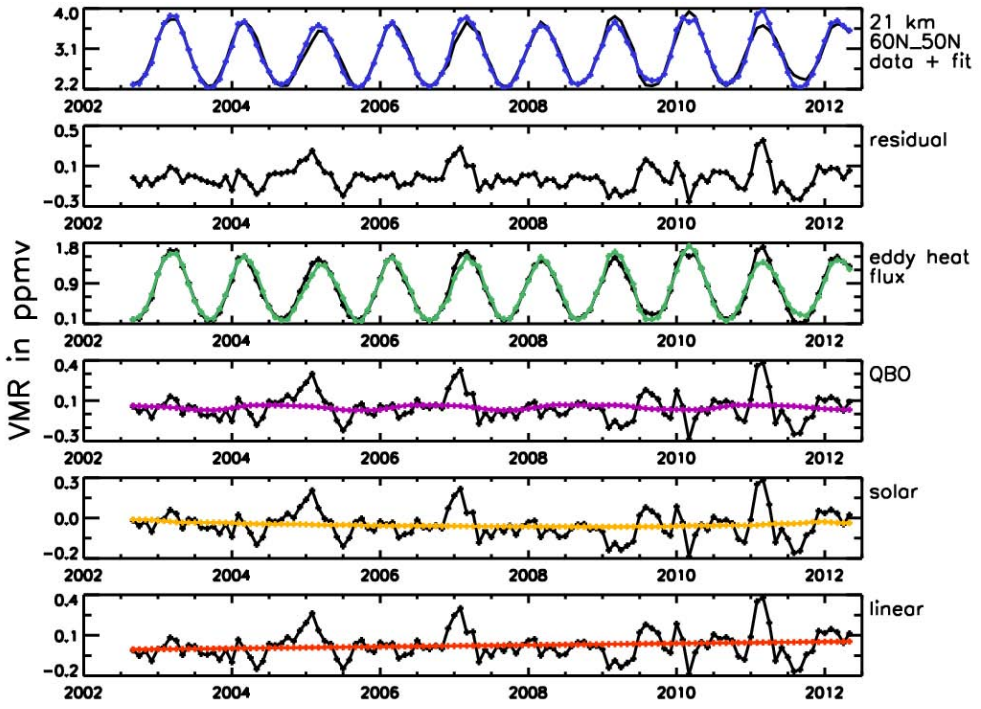

Fig. 1. Time series of the O_3 mixing ratio from SCIAMACHY at 21 km for 60–50° N (blue) with overlaid fitting curve (black) in top panel and fit residuals (second panel). Below, the components of the fitting curve are shown individually (from top to bottom): cumulative eddy heat flux (green), QBO (magenta), solar cycle (orange), and linear change (red). Each of these terms is overlaid by the time series with all other components of the fitting curve subtracted, e.g. the eddy heat flux terms by the time series with QBO, solar cycle, and linear terms subtracted.

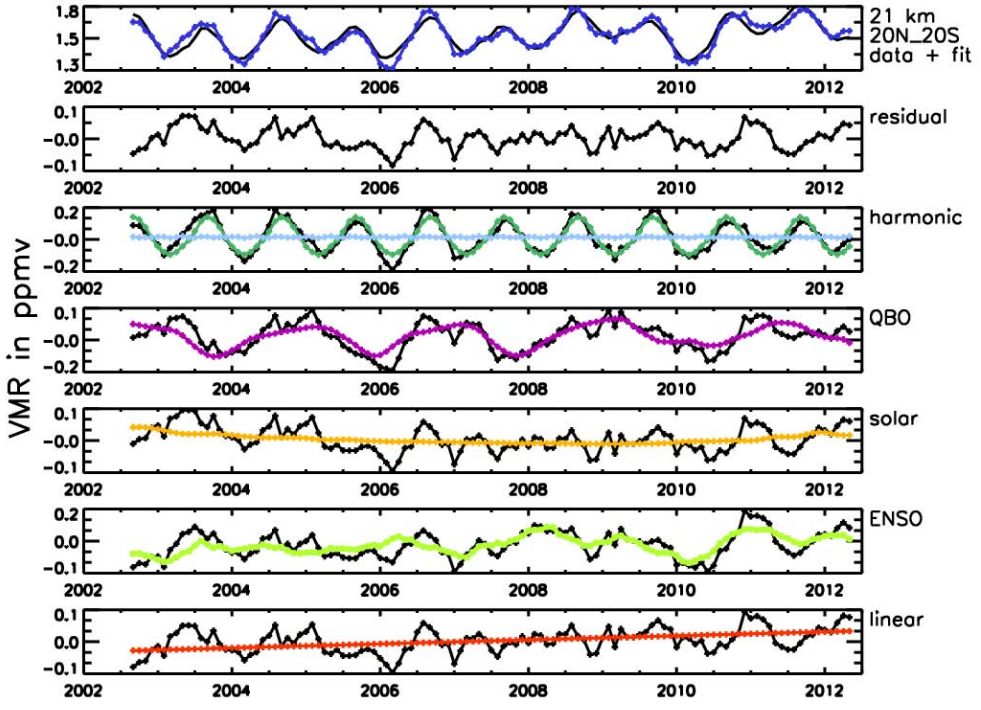

Fig. 2. Same as Fig. 1 but for 20° N–20° S and with ENSO terms included (last but one panel, bright green curve). Here, the third panel shows harmonic terms, both comprising all periods used, i.e. 12, 6, 4, and 3 months (green), and as a combination of the terms with 4- and 3-month periods only (light blue).

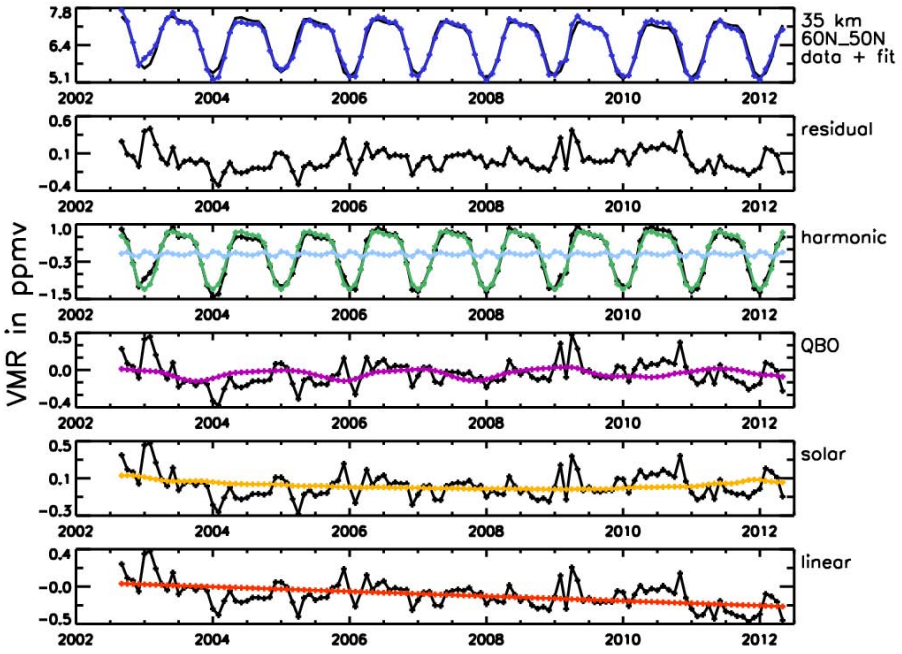

Fig. 3. Same as Fig. 1 but for 35 km altitude. Third panel as in Fig. 2: harmonics as seasonal terms.

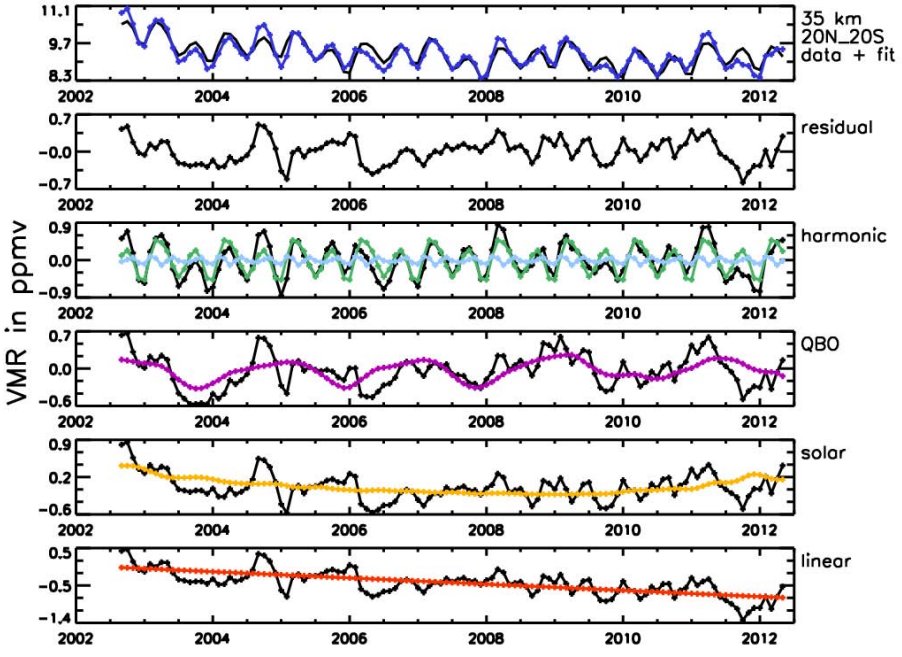

Fig. 4. Same as Fig. 1 but for 35 km altitude and 20° N–20° S. Third panel as in Fig. 2: harmonics as seasonal terms.

of tropical O_3 in the lowermost tropical stratosphere which is driven by effects related to the tropical upwelling (Randel et al., 2007). At 35 km in the tropics, the QBO and semi-annual terms dominate the periodic variability of O_3. As discussed before, the maximum QBO response of tropical O_3 is located within around 20–27 km and 30–38 km. At 44 km in the tropics, the semi-annual terms provide the most important contribution to the fitting curve. In the middle tropical stratosphere, the semi-annual oscillation of O_3 is driven by photochemical O_3 production, which reflects two Equator passages of the Sun per year (Perliski et al., 1989).

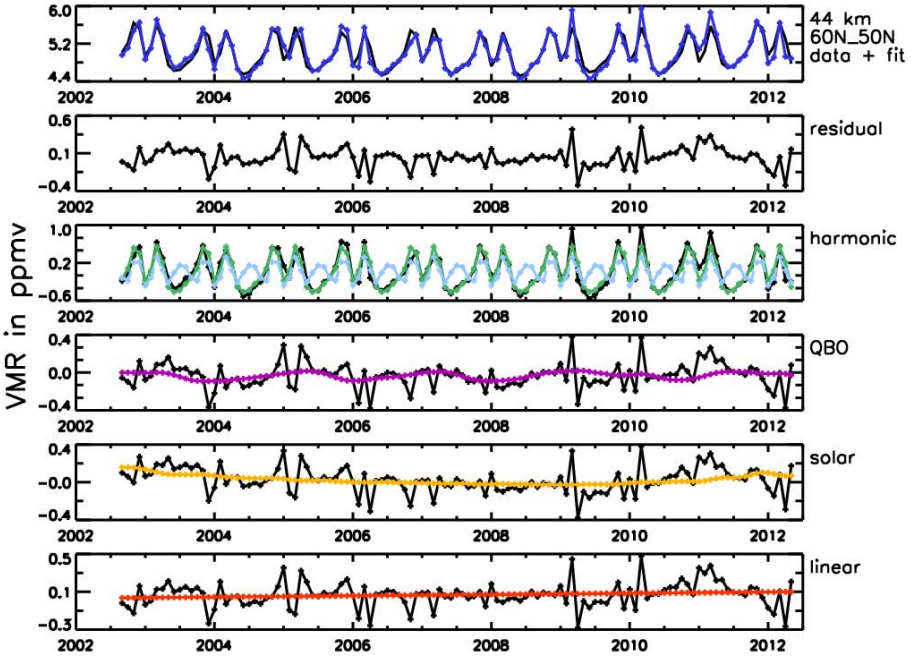

Fig. 5. Same as Fig. 1 but at 44 km altitude. Third panel as in Fig. 2: harmonics as seasonal terms.

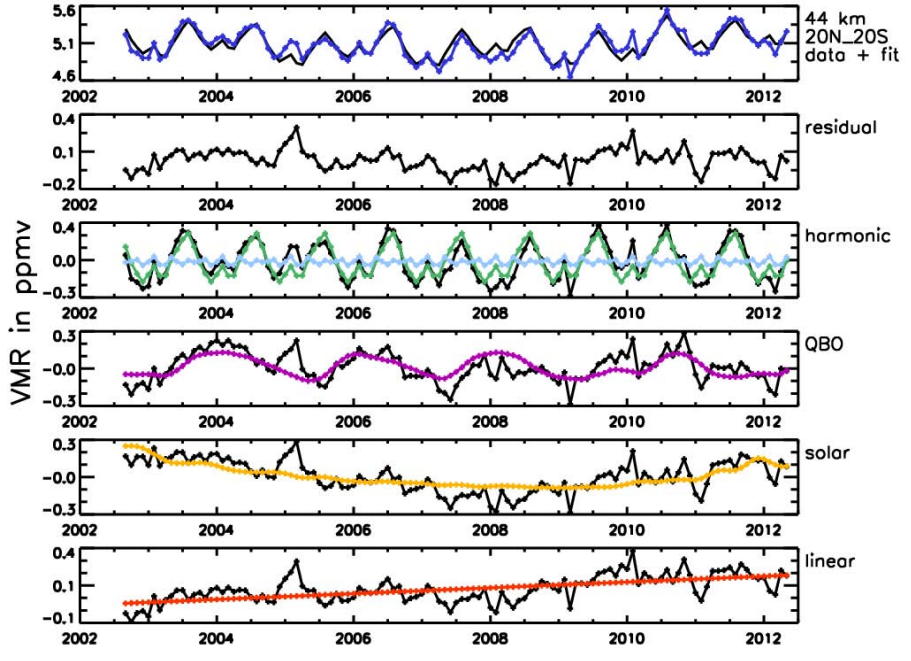

Fig. 6. Same as Fig. 1 but for 44 km altitude and 20° N–20° S. Third panel as in Fig. 2: harmonics as seasonal terms.

5 Ozone trends from SCIAMACHY

O_3 trend profiles and estimated uncertainties (both in % dec^{-1}) are shown in Fig. 7 for the period of August 2002–April 2012. The underlying latitude bands are 60–50° N and 50–60° S (midlatitudes) and 20° N–20° S (tropics). The following features of particular interest are readily identified:

- double-peak structure of positive trend in the tropics below 30 km (having two maxima at values close to 5 % dec^{-1} between 20 and 30 km)
- single-peak structure of negative trend in the tropics between 30 and 38 km (maximising at 33–34 km at a value of around -10 % dec^{-1})

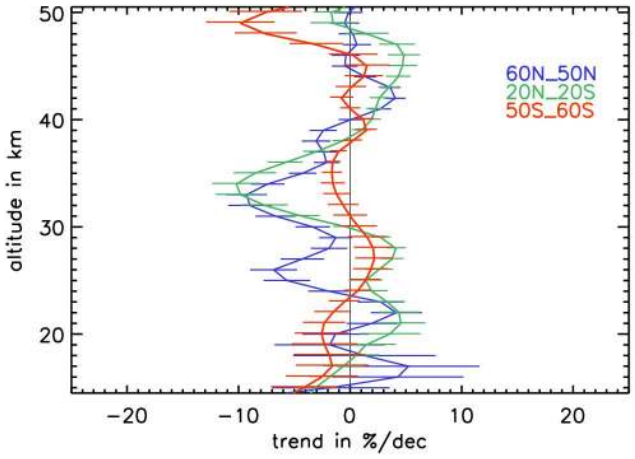

Fig. 7. Ozone trend profiles inferred from SCIAMACHY limb measurements for the latitude bands 60–50° N, 20° N–20° S, and 50–60° S, August 2002–April 2012. Error bars: 1σ.

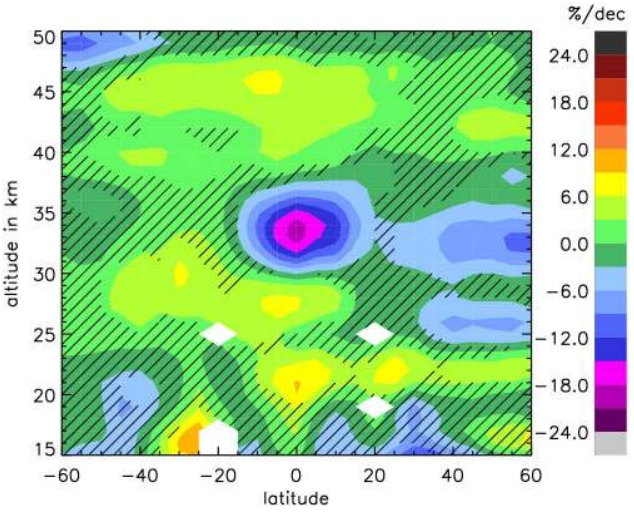

Fig. 8. Latitude–altitude plot of ozone trends from SCIAMACHY: latitude range from 60° N to 60° S, altitude range from 15 to 50 km. Non-hatched are significances at the 2σ level. August 2002–April 2012. Legend on the right: units of % dec^{-1}.

- positive trends in the upper tropical stratosphere between 39 and 47 km and at northern midlatitudes (between 40 and 45 km) of around 5 % dec^{-1}
- hemispheric asymmetry of trends at midlatitudes between 25 and 35 km: negative trends in the north and zero to positive trends in the south maximising at values of around -10 % dec^{-1} and 3 % dec^{-1} respectively.

In the 35–45 km range of 50–60° S, the trends are relatively close to zero and become increasingly negative above 45 km. The trend errors are comparable for all three latitude bands.

A stability check was performed for the O_3 trend profiles from SCIAMACHY by shifting the starting point of the underlying time series forward in time in 6-month steps, i.e. from August 2002 to February 2003, from February 2003 to August 2003, from August 2003 to February 2004, and from February 2004 to August 2004. In all cases, the trends and their uncertainties are well replicated and the overall shape of vertical trend profiles is conserved for the three latitude bands. It is, however, essential to extend the period to 2011. Otherwise, the solar cycle terms reflect mainly the descending branch of the solar cycle and may interfere with the linear trend. This may, in turn, result in larger trend uncertainties. Practically no change of the vertical trend profiles from SCIAMACHY results if omitting data from the year 2012, i.e. confining the time range of trend calculation to August 2002–December 2011.

Figure 8 shows a latitude–altitude plot of the O_3 trends spanning the latitude range from 60° N to 60° S. The plot is based on zonally averaged O_3 data in 5° latitude steps, defined by the data gridding described in Sect. 2. As a function of the latitude, the trends are shown for the 15 to 50 km altitude range. As evidenced before for the 20° N–20° S tropical latitude band, there are double-peaked positive trends below 30 km (significant at their maxima at around 21 km and between 25 and 30 km) and single-peaked negative trends between 30 and 38 km in the inner tropics. In the 30–35 km range, an "island" of significant negative O_3 trends of up to -20 % dec^{-1} now appears. At latitudes from 20° N to 30° N, significant positive trends are seen at altitudes between 20 and 25 km. Positive trends in the upper stratosphere (identified in Fig. 7 for 20° N–20° S between 39 and 47 km and also for 60–50° N between 40 and 45 km) are observed over large parts of the latitude range from 60° N to 60° S. These trends are mostly significant at values of around 5 % dec^{-1}. The hemispheric asymmetry at midlatitudes between 25 and 35 km is clearly pronounced with significant negative trends in the Northern Hemisphere and significant positive trends in the Southern Hemisphere. At around 15 km, positive trends appear between 20° S and 30° S. These trends should, however, be treated with caution because of potential impact of clouds at altitudes below 20 km (Mieruch et al., 2012).

A discussion of the latitude and altitude dependence of the QBO and solar cycle responses as seen by SCIAMACHY limb is presented in Appendix A.

6 Comparisons of trends from SCIAMACHY with those from other instruments

6.1 OSIRIS/Odin

The Odin satellite, which carries the OSIRIS instrument (Llewellyn et al., 2004), follows a near-terminator orbit so that the illumination conditions specific to OSIRIS are always close to the solar terminator. The ascending node was

between 6 and 7 p.m. over the time span considered here. Similar to SCIAMACHY, OSIRIS measures the scattered solar light in limb-viewing geometry. Seasonal variations of day- and nighttime interrupt the OSIRIS measurements in the winter hemisphere. As a result, OSIRIS provides continuous time series only in the tropics. The data might also be inhomogeneously distributed around the Equator, i.e. predominantly to the north from it during northern summer and vice versa. Thus, the comparison between the instruments is performed for the tropical 20° N–20° S latitude band only.

The OSIRIS O_3 data, used in this study, are from the retrieval version 5.07 produced by the University of Saskatchewan, which has a modified filtering of outliers with respect to earlier versions. The OSIRIS data separate clearly into records at a.m. and p.m. local time. As pointed out by Huang et al. (2010), diurnal variations of O_3 are expected to be on the order of only a few percent in the stratosphere. The AM Equator crossing time of Odin is closer to the Equator crossing of ENVISAT at daylight. Accordingly, the a.m. data from OSIRIS, which are closer in local time to the data from SCIAMACHY, are used in the following (without any correction for diurnal variation).

The retrieval altitudes of OSIRIS and SCIAMACHY lie between one another. For each altitude of SCIAMACHY from 15 to 50 km, the O_3 values from the adjacent altitudes of OSIRIS were interpolated.

The instrument comparison between SCIAMACHY and OSIRIS (also between SCIAMACHY and EOS MLS as described in Sect. 6.2) uses zonal monthly mean data. As mentioned in Sect. 2, a comparison of zonal monthly means from gridded data is considered an equivalent alternative to the use of collocated data. As a further check, the trend profiles from SCIAMACHY and OSIRIS (comparison described in Sect. 6.4) were tested to remain practically unchanged when using collocated measurements.

6.2 EOS MLS

The MLS instrument aboard the EOS Aura satellite (Jarnot et al., 2006) measures the thermal radiation emitted by the Earth's atmosphere in the microwave spectral range on both the day and night side of the near-polar orbit. MLS went into routine operation in August 2004. In this comparison, we have used O_3 profiles retrieved from MLS daytime measurements. Aura crosses the Equator in ascending node at 13:45 local time. Its daytime measurements extend deep into both hemispheres similar to those from SCIAMACHY. Thus, the comparison between the instruments is also done at midlatitudes, represented by the latitude bands of 60–50° N and 50–60° S. The period used for the comparison is August 2004–April 2012.

In accordance with the recommendations from the MLS team, the MLS O_3 data used here are from the retrieval version 2.2. The pressure serves as the vertical coordinate in version 2.2. After conversion from pressure to geometric height, the MLS O_3 profiles are interpolated at the altitudes of the SCIAMACHY retrieval. Zonal monthly means are calculated between 15 and 50 km.

6.3 SHADOZ ozonesondes

Balloon-borne in situ measurements of ozonesondes are also used for a comparison with the O_3 trend from SCIAMACHY limb. The altitude range of the balloon sonde O_3 data is limited to 30–35 km by different factors, such as balloon burst and evaporation and/or freezing of the wet-chemical sensing solution used in the sondes. The data from ozonesondes have a vertical resolution on the order of 100 m, clearly finer than that from satellite instruments. For the comparison, the vertical O_3 profiles from the sondes are smoothed over intervals of ± 2 km relative to altitudes defined by the O_3 retrieval from SCIAMACHY, i.e. from 15 to 30 km in steps of 1 km. In the following, these smoothed O_3 profiles are used to determine monthly averaged O_3 time series from the sondes.

SHADOZ is a network of more than 10 ozonesonde stations at (sub)tropical sites (e.g. Thompson, 2003). Since coming into being in 1998, the network has been systematically operational with typically several ozonesonde launches per month per station. The datasets of all stations are freely accessible via http://croc.gsfc.nasa.gov/shadoz/. Here, we select the inner-tropical stations at Ascension (8.0° S, 14.4° W), Kuala Lumpur (2.7° N, 101.7° E), Nairobi (1.3° S, 36.8° E), Natal (5.4° S, 35.4° W), and Paramaribo (5.8° N, 55.2° W). These stations are relatively equidistant in latitude (less importance is attached to their longitudes as tropical stratospheric O_3 is known to be highly zonally symmetric). The monthly averaged O_3 time series over all 5 stations are calculated. In order to account for possible offsets between the stations, the mean values of single-station time series are forced to be equal before averaging. The is done by shifting them so that a reference value is matched. This reference value is the mean value of one of the stations, in our case Paramaribo (arbitrarily selected). The resulting sonde trend profile is compared to the trend profile from SCIAMACHY, which is based on data selected at latitudes and longitudes around the sites of the ozonesonde stations and averaged accordingly.

6.4 Comparison results

SCIAMACHY vs. OSIRIS and MLS

Figures 9 and 10 show the comparison between SCIAMACHY and MLS at midlatitudes for the period August 2004–April 2012. At northern midlatitudes, the MLS O_3 trend profile has less variability with altitude than that of SCIAMACHY. There are some significant deviations between 30 and 35 km, with SCIAMACHY showing negative trends while MLS shows small positive trends. Positive trends seen by SCIAMACHY around 40 to 45 km agree with

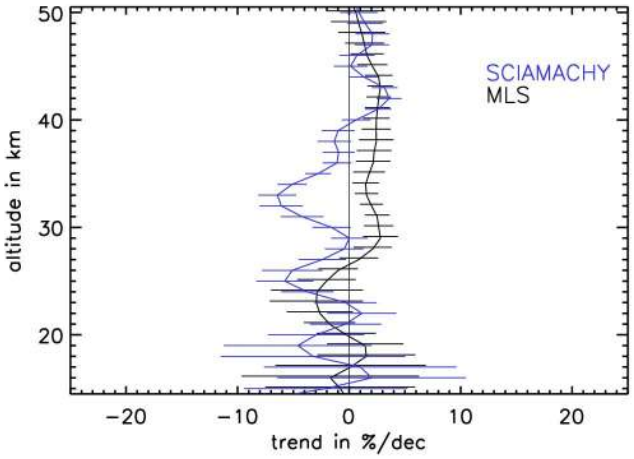

Fig. 9. Comparison of ozone trends inferred from SCIAMACHY and MLS measurements: 60–50° N, August 2004–April 2012. Error bars: 1σ.

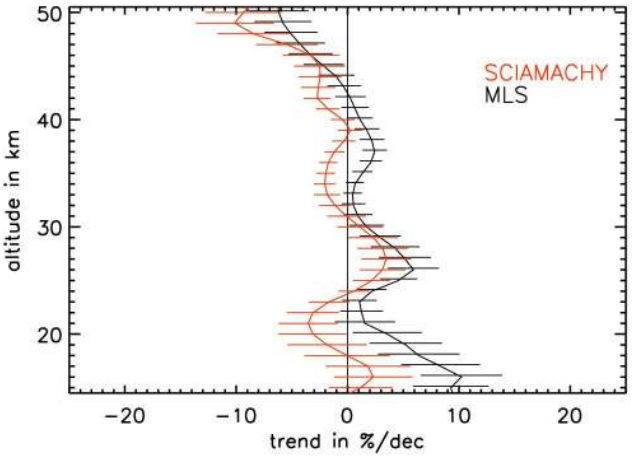

Fig. 10. Comparison of ozone trends inferred from SCIAMACHY and MLS measurements: 50–60° S, August 2004–April 2012. Error bars: 1σ.

MLS. There is also reasonable agreement at southern mid-latitudes. The trend profiles from both instruments follow each other closely and have similar error bars. The agreement between SCIAMACHY and MLS holds up to 50 km, where both profiles become increasingly negative.

Tropical O_3 trends from SCIAMACHY, OSIRIS, and MLS are compared in Fig. 11. The tropics are represented by the latitude band of 20° N–20° S, and the time span from August 2004 to April 2012 is selected for the comparison. In qualitative agreement, SCIAMACHY, OSIRIS, and MLS show negative trends between 30 and 35 km. SCIAMACHY reaches around $-10\,\%\,\mathrm{dec}^{-1}$, while the trends from OSIRIS are around $-4\,\%\,\mathrm{dec}^{-1}$ at maximum. The trends from MLS lie between those from SCIAMACHY and OSIRIS.

Between 25 and 30 km, the O_3 datasets from all three instruments show in good agreement positive trends. Agreement within the trend uncertainties is achieved down to around 20 km. In the UTLS region, the trends from SCIAMACHY and OSIRIS change from moderately positive at 20 km to moderately negative at 15 km, while MLS increases to 10–20 $\%\,\mathrm{dec}^{-1}$ (which is consistent with the results from SHADOZ; see following subsection). Between around 38 and 46 km, both SCIAMACHY and OSIRIS show positive trends. Trends up to around $6\,\%\,\mathrm{dec}^{-1}$ are obtained from SCIAMACHY near 45–46 km and from OSIRIS around 40 km. Contrastingly, the trends from MLS are zero to negative above 40 km. Above 48 km, zero to slightly negative O_3 trends are shown by all compared instruments. Taken as a whole, the shape of the trend profile of tropical O_3 identified from SCIAMACHY in Sect. 5 is confirmed by both OSIRIS and MLS.

SCIAMACHY vs. SHADOZ

Figure 12 compares the SHADOZ sonde and SCIAMACHY O_3 trend profiles from 15 to 30 km. Though it is derived from data averaged over latitudes and longitudes matching the sites of ozonesonde stations, the trend profile from SCIAMACHY resembles well the trend pattern derived from zonal averages at latitudes from around 5° N to 5° S in Fig. 8. This is a result of the high zonal symmetry of tropical O_3 (Thompson, 2003; Randel and Thompson, 2011). The trend profile from SCIAMACHY shows zero to positive trends between 15 and 30 km. Good agreement to the positive trends seen by the sondes is obtained between 18 and 29 km. Below 18 km, the trends from the sondes climb towards a maximum while the trends from SCIAMACHY decay towards zero. The differences between 15 and 20 km may arise from the satellite retrieval suffering from the impacts of high convective clouds; see e.g. Mieruch et al. (2012).

7 Discussion of factors potentially explaining the O_3 trends observed

The O_3 trend profiles from SCIAMACHY and the comparison instruments tend to have non-negative trends in the tropical 17–20 km range. Constraining our study of trends to the 2002 to 2012 decade, this behaviour is in contrast to the results obtained by Randel and Thompson (2011). Their O_3 trends were inferred from a dataset merged between SAGE II and SHADOZ spanning the time range of 1984–2009. Negative trends were identified in the lowermost tropical stratosphere and attributed to enhanced tropical upwelling.

In the tropical stratosphere below 30 km, both changing dynamics and chemical composition potentially explain the positive O_3 trends observed by SCIAMACHY. For example, changes in the rate of tropical upwelling, changes in

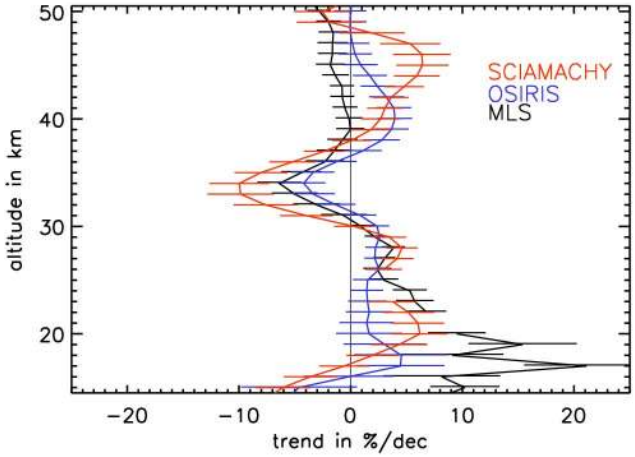

Fig. 11. Comparison of ozone trends inferred from SCIAMACHY, MLS, and OSIRIS measurements: 20° N–20° S, August 2004–April 2012. Error bars: 1σ.

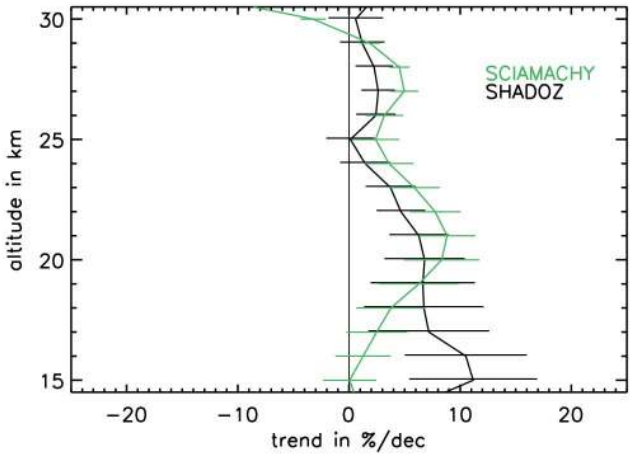

Fig. 12. Comparison of ozone trends inferred from SCIAMACHY and from an average of tropical SHADOZ ozonesonde stations including Ascension (8.0° S, 14.4° W), Kuala Lumpur (2.7° N, 101.7° E), Nairobi (1.3° S, 36.8° E), Natal (5.4° S, 35.4° W), and Paramaribo (5.8° N, 55.2° W). The data from SCIAMACHY are selected at latitudes and longitudes close to the sites of the ozonesonde stations and averaged accordingly. The considered period is August 2002–April 2012. Error bars: 1σ.

the amount of halogens, or changes in the NO_X amount are possibly responsible for changes in O_3. Analysing O_3 partial columns between 18 and 25 km, Yang et al. (2006) found that halogens are of minor importance in this altitude range because CFCs do not release radicals immediately after their injection through the tropical tropopause. Since the vertical gradient of O_3 is positive, enhanced vertical advection has a negative O_3 response in the lower tropical stratosphere. Randel and Thompson (2011) suggested that an increase of the tropical upwelling has led to negative O_3 trends around 17 to 21 km observed over the period 1984–2009. As the O_3 trends seen by SCIAMACHY and the comparison instruments are non-negative at this altitude range and become clearly positive between 25 and 30 km, they must have another explanation. According to Nevison et al. (1999), an increase in NO_X might be a reason for a positive trend in O_3 at these altitudes. This is because NO_X is involved in buffering effects as a result of interactions with HO_X and ClO_X beside catalytic O_3 depletion. Nevison et al. (1999) have shown that an increase in NO_X results in an O_3 enhancement extending up to around 30 km in the proximity of the Equator. As noted by Burrows et al. (1979), NO_X may also catalytically produce O_3 in the lowermost stratosphere. The altitude range below 30 km coincides with the positive O_3 trends observed in our study. As also follows from Nevison et al. (1999), increasing NO_X may lead to O_3 decreases above 30 km. Accordingly, increasing NO_X may contribute to the negative O_3 trends seen by SCIAMACHY in the tropical 30–38 km range as well. However, the anthropogenic increase of NO_X assumed in Nevison et al. (1999) results in a decrease of around 1 % per decade in tropical midstratospheric O_3, which cannot explain the observed negative trends of -4 to $-10\,\%\,\mathrm{dec}^{-1}$ inferred in our study (cf. Fig. 11). Thus, the correlation between O_3 and NO_X pointed out by Nevison et al. (1999) can explain the observed trends only if sources of NO_X other than anthropogenic emissions exist. An investigation of the possible sources of NO_X is beyond the scope of this study. Further research is needed on this issue.

Positive O_3 trends of approximately $5\,\%\,\mathrm{dec}^{-1}$ are inferred from SCIAMACHY in the upper stratosphere over large parts of the tropics and midlatitudes. As O_3 in the upper stratosphere is highly sensitive to halogens (WMO, 1999), these trends are favoured to reflect declining halogens. Evidence for a turnaround in upper stratospheric O_3 has already been pointed out by Reinsel (2002). Some attribution to declining halogens has been provided by Newchurch et al. (2003). Their study is based on satellite data indicating at least a levelling-off of O_3 in the tropics and extratropics. Meanwhile the O_3 abundance continuing some levelling-off or slightly increasing is supported by various ground-based lidar and microwave radiometer stations (Steinbrecht et al., 2006, 2009).

A potential explanation for some of the O_3 trends obtained as a function of latitude and altitude is provided by Eckert et al. (2013) based on MIPAS/ENVISAT O_3 data covering the same observation period as SCIAMACHY. A hypothetical shift of subtropical mixing barriers is theorised to result in negative trends in the northern extratropics and positive trends in the southern extratropics. This pattern of trends is similar to the asymmetry between the northern and southern trend profiles from SCIAMACHY between 25 and 35 km. In addition, positive/negative O_3 trends in the lower/middle tropical stratosphere are theorised by Eckert et al. (2013), although the tropical trends from SCIAMACHY partly are more pronounced and somewhat different in altitude. This

explanation, if correct, implies that the subtropical mixing barriers having undergone shifts during the last decade may contribute to the tropical O_3 trends observed in our study.

8 Potential instrumental and algorithmic issues

As discussed by von Savigny et al. (2005), pointing misalignment is one of the major error sources for limb-viewing instruments on ENVISAT. A robust method for determining tangent height offsets from solar occultation measurements of SCIAMACHY has been developed by Bramstedt et al. (2012). Using this method, tangent height offsets on the order of few hundred metres were identified. The overall behaviour of the pointing misalignment is mainly governed by constant and seasonally varying components. In addition, a continuous drift of the pointing misalignment on the order of 50 m throughout the first four years of the SCIAMACHY mission and no drift thereafter were identified. While any possible artefacts due to constant and seasonally varying components are neutralised by the corresponding regression terms and hence are not expected to produce trend errors, the influence of the continuous drift on the resulting trends needs to be further investigated. Assuming similar pointing drifts for both limb and occultation measurements, this is done by calculating the trends for drift-corrected time series. The weighting functions of the vertical profile of O_3 with respect to the pointing offset needed to perform the correction are calculated numerically using one representative profile for each season. The corrected time series yield up to 1 % dec^{-1} lower O_3 trends in the 40–50 km range and practically the same results as uncorrected elsewhere.

As described in Sect. 6.4, negative O_3 trends from SCIAMACHY observed between 30 and 38 km in the tropics are qualitatively confirmed by both EOS MLS and OSIRIS/Odin, but the comparison instruments show less negative trends than SCIAMACHY. This altitude range is known to be possibly affected by reduced sensitivity in the SCIAMACHY retrieval resulting from a transition between the retrieval information coming from UV and visible wavelengths. Previously, positive offsets in SCIAMACHY O_3 number densities compared to the datasets from other instruments were observed in the tropics around 30 km and around 40 km by Mieruch et al. (2012). Similarly, compared to a variety of satellite instruments in Tegtmeier et al. (2013), SCIAMACHY has 10–20 % higher O_3 mixing ratios in the tropics around 10 hPa, which is close to 30 km in altitude. In addition, the QBO amplitude seen by SCIAMACHY lies above the multi-instrument average in the middle tropical stratosphere. However, the QBO amplitude, if overestimated, is not necessarily a source of error for trends as QBO signals influence mainly trend uncertainties. As a result of the inclusion of QBO terms into the regression model used in this study, trend uncertainties of SCIAMACHY are clearly reduced in the middle and lower tropical stratosphere while trend values remain practically unchanged. Furthermore, analysing long-term time series, Tegtmeier et al. (2013) found no indications for temporal instability of the SCIAMACHY instrument.

As pointed out by Jones et al. (2009) and McLinden and Fioletov (2011), O_3 trends can differ dependent on the physical units used for ozone and the vertical coordinate (VMR versus number density, pressure versus geometric height) due to possible trends in the neutral density (temperature and pressure) that is needed for unit conversion. Our investigation shows that the O_3 trends in number density units, obtained from EOS MLS measurements using their own pressure and temperature information, agree better with SCIAMACHY in the tropical 30–40 km range, while no significant changes are observed below 30 km (not shown). However, converting number density into volume mixing ratio does not alter the ozone trends for OSIRIS/Odin and SCIAMACHY. This suggests that the neutral density trends derived from ECMWF data and those obtained from MLS are significantly different at these altitudes. Both SCIAMACHY and OSIRIS do not retrieve temperature (unlike MLS), and, therefore, ECMWF operational temperatures are used in the retrieval and unit conversion. As pointed out by Adams et al. (2013), drifts in the meteorological data can also affect ozone trends when units are converted. In our study, a significant disagreement above 35 km was identified when comparing the neutral density trends obtained from ECMWF operational and ERA-Interim datasets (not shown here).

9 Conclusions

Rates of linear change or trends were determined for stratospheric O_3 in the 15–50 km range for the time range August 2002 to April 2012. In the tropics (20° N–20° S), the O_3 trends from SCIAMACHY are found to be positive in the lower stratosphere and negative in the middle stratosphere. The positive trends maximise between 20 and 30 km, are double-peaked, and maximise at values close to 5 % dec^{-1}. The negative trends are single-peaked and maximise at 33–34 km at values of around -10 % dec^{-1}. The observed trends at this altitude are about twice the trends observed by OSIRIS (this paper), MIPAS (Eckert et al., 2013), and the combined SAGE II/GOMOS (Kyrölä et al., 2013).

As suggested by Nevison et al. (1999), increasing NO_X may contribute both to the positive O_3 trends observed below 30 km and the negative O_3 trends observed above 30 km in the tropics. In the upper stratosphere between around 40 and 47 km, positive O_3 trends of around 5 % dec^{-1} are seen by SCIAMACHY from the tropics to the midlatitudes of both hemispheres. These trends are believed to be in response to declining halogens as this region is highly sensitive to halogen chemistry (WMO, 1999). Similar O_3 trends have been previously reported by Steinbrecht et al. (2006, 2009), Jones et al. (2009), and WMO (2011) in the 35–45 km range.

For the latitude band of 20° N–20° S, representing the tropics, O_3 trends have been compared between SCIAMACHY, OSIRIS/Odin, and EOS MLS. In addition, a trend comparison between SCIAMACHY and SHADOZ ozonesondes has been made within the inner tropics. For the latitude bands of 60–50° N and 50–60° S, representing the midlatitudes, trends have been compared between SCIAMACHY and EOS MLS. The trends from SCIAMACHY and the comparison instruments are found to be in reasonable agreement down to altitudes around 20 km. The shape of tropical O_3 trends identified from SCIAMACHY is overall well confirmed by all comparison instruments. In the lowermost tropical stratosphere below 20 km, SCIAMACHY and the comparison instruments see non-negative trends but do not agree in detail. The other instruments show higher positive trends than SCIAMACHY.

Appendix A

QBO and solar cycle variability as seen by SCIAMACHY

The QBO proxies, the 10 hPa and 30 hPa Singapore winds, are phase-shifted by approximately a quarter of a period. This combination can be roughly approximated by the sum of a sine and a cosine term with an effective frequency

$$A\sin(\omega t+\phi) = A\cos(\omega t)\sin\phi + A\sin(\omega t)\cos\phi = \quad \text{(A1)}$$
$$= a\cos(\omega t) + b\sin(\omega t).$$

The phase constant is given by $\phi = \arctan(\frac{a}{b})$. For $t = 0$, this yields

$$A\sin\phi = a, \quad \text{(A2)}$$

or

$$A = \frac{a}{\sin(\arctan(\frac{a}{b}))}. \quad \text{(A3)}$$

Determining the QBO amplitude by this approach, a and b are given by the fit coefficients of the QBO proxies (cf. Eq. 3).

The inferred QBO amplitude from SCIAMACHY limb O_3 is shown in Fig. A1 as a function of altitude and latitude. At equatorial latitudes, a maximum amplitude is obtained at altitudes of 25–28 km and 30–36 km. This pattern of maximum amplitude is consistent with the vertical structure of the QBO response of tropical O_3 described in Sect. 3.2. Both the spatial distribution and the strength of the inferred amplitude are in close agreement with MIPAS/ENVISAT observations as shown by Eckert et al. (2013) who used a similar approach. The maximum of SCIAMACHY QBO amplitude of around 0.6 ppmv at around 33 km is larger than MIPAS values by a factor of around 1.5. This is consistent with findings by Tegtmeier et al. (2013). Comparing QBO signatures measured by a variety of instruments, it was shown that the QBO amplitude from SCIAMACHY lies above the multi-instrument

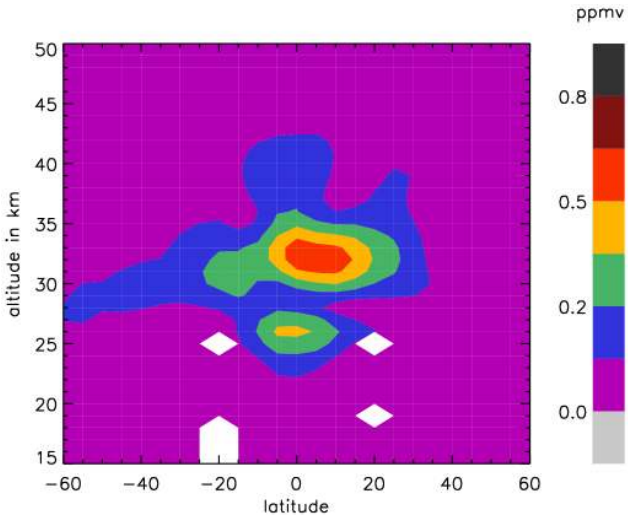

Fig. A1. Latitude–altitude plot of the amplitude of the QBO response of O_3 as seen by SCIAMACHY: latitude range from 60° N to 60° S, altitude range from 15 to 50 km. August 2002–April 2012. Legend on the right: units of ppmv.

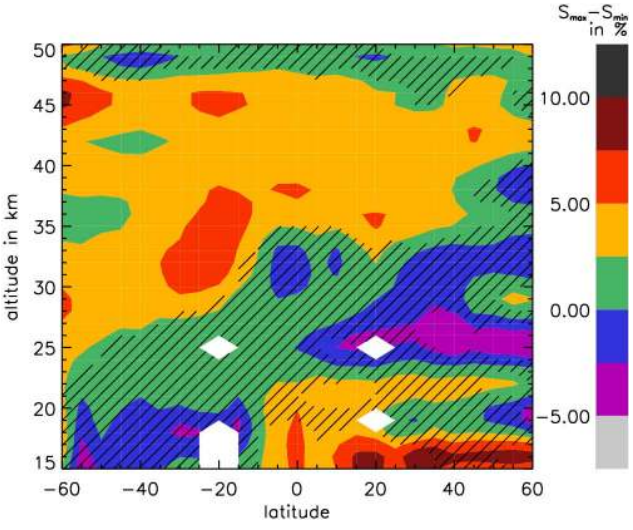

Fig. A2. Latitude–altitude plot of solar cycle signal in SCIAMACHY limb O_3: latitude range from 60° N to 60° S, altitude range from 15 to 50 km. Significances at the 2σ level are non-hatched areas. The solar cycle signal is expressed as the solar max minus min change of O_3 (more detailed explanation in the text). It is scaled in relative units with respect to the mean value of the underlying time series. The period of August 2002–April 2012 is considered. Legend on the right: solar max minus min change in units of %.

average, while MIPAS/ENVISAT exhibits a QBO amplitude lower than average.

Some altitude dependence is also discernible in the solar cycle signal of O_3, obtained from the use of the Mg II index as solar cycle proxy, shown in Fig. A2. For the Mg II

index, a change of 0.01 between solar maximum and minimum is assumed (this is considered to be a realistic estimate of the difference between the maximum of solar cycle 24 and the minimum at the end of solar cycle 23). Scaling the maximum minus minimum change of the proxy by its regression coefficient yields the corresponding solar max minus min change in O_3. Here, it is expressed in relative units (with respect to the mean value of the underlying time series). For large parts, the solar cycle signal is significant at the 2σ level at altitudes between 35 and 45 km and insignificant below and above. Analysing a merged satellite dataset from 1984–2011, the study of Kyrölä et al. (2013) inferred a largely similar distribution of significances for the solar cycle signal. The strength of their solar cycle signal being lower than ours by a factor up to 2 may be partly explained by the difference in the analysed time span and/or scaling the solar cycle signals in relative units with respect to the constant term of their regression (not the mean value of the underlying time series).

Acknowledgements. This research was funded in part by the German Research Foundation (DFG) through the Freie Universität Berlin within the Research Unit SHARP (FOR 1095), subproject OCF, the State and University of Bremen, the DLR within the project SADOS (50EE1105), and the ESA within the project CCI Ozone. The retrieval of the O_3 data uses pressure and temperature information from the operational analysis data from the European Centre for Medium-Range Weather Forecasts (ECMWF). We also would like to acknowledge the local support of H. Schröter in setting up and running the retrieval scripts. We are grateful to the processing teams of EOS-MLS, OSIRIS, and SHADOZ for providing us with their data products. We thank N. V. Balashov (Pennsylvania State University) for communications about SHADOZ details. Research at the Jet Propulsion Laboratory, California Institute of Technology, was carried out under contract with the National Aeronautics and Space Administration.

Edited by: J. Urban

References

Adams, C., Bourassa, A. E., Sofieva, V., Froidevaux, L., McLinden, C. A., Hubert, D., Lambert, J.-C., Sioris, C. E., and Degenstein, D. A.: Assessment of Odin-OSIRIS ozone measurements from 2001 to the present using MLS, GOMOS, and ozone sondes, Atmos. Meas. Tech. Discuss., 6, 3819–3857, doi:10.5194/amtd-6-3819-2013, 2013.

Baldwin, M. P., Gray, L. J., Dunkerton, T. J., Hamilton, K., Haynes, P. H., Randel, W. J., Holton, J. R., Alexander, M. J., Hirota, I., Horinouchi, T., Jones, D. B. A., Kinnersley, J. S., Marquardt, C., Sata, K., and Takahashi, M.: The quasi-biennial oscillation, Rev. Geophys., 39, 179–229, doi:10.1029/1999RG000073, 2001.

Bovensmann, H., Burrows, J. P., Buchwitz, M., Frerick, J., Noël, S., Rozanov, V. V., Chance, K. V., and Goede, A. P. H.: SCIAMACHY: Mission Objectives and Measurement Modes, J. Atmos. Sci., 56, 127–150, 1999.

Bramstedt, K., Noël, S., Bovensmann, H., Gottwald, M., and Burrows, J. P.: Precise pointing knowledge for SCIAMACHY solar occultation measurements, Atmos. Meas. Tech., 5, 2867–2880, doi:10.5194/amt-5-2867-2012, 2012.

Burrows, J. P., Cliff, D. I., Harris, G. W., Thrush, B. A., and Wilkinson, J. P. T.: Atmospheric reactions of the HO_2 radical studied by laser magnetic resonance, P. R. Soc. A, 368, 463–481, 1979.

Burrows, J. P., Hölzle, E., Goede, A. P. H., Visser, H., and Fricke, W.: SCIAMACHY – Scanning Imaging Absorption Spectrometer for Atmospheric Chartography, Acta Astronaut., 35, 445–451, 1995.

Butchart, N., Scaife, A. A., Austin, J., Hare, S. H. E., and Knight, J. R.: Quasi-biennial oscillation in ozone in a coupled chemistry-climate model, J. Geophys. Res., 108, 4486, doi:10.1029/2002JD003004, 2003.

Chipperfield, M. P., Gray, L. J., Kinnersley, J. S., and Zawodny, J.: A Two-Dimensional Model Study of the QBO Signal in SAGE II NO_2 and O_3, Geophys. Res. Lett., 21, 589–592, doi:10.1029/94GL00211, 1994.

Cochrane, D. and Orcutt, G. H.: Application of least squares regression to relationships containing autocorrelated error terms, J. Amer. Stat. Assoc., 44, 32–61, 1949.

Dhomse, S., Weber, M., Wohltmann, I., Rex, M., and Burrows, J. P.: On the possible causes of recent increases in northern hemispheric total ozone from a statistical analysis of satellite data from 1979 to 2003, Atmos. Chem. Phys., 6, 1165–1180, doi:10.5194/acp-6-1165-2006, 2006.

Eckert, E., von Clarmann, T., Kiefer, M., Stiller, G. P., Lossow, S., Glatthor, N., Degenstein, D. A., Froidevaux, L., Godin-Beekmann, S., Leblanc, T., McDermid, S., Pastel, M., Steinbrecht, W., Swart, D. P. J., Walker, K. A., and Bernath, P. F.: Drift-corrected trends and periodic variations in MIPAS IMK/IAA ozone measurements, Atmos. Chem. Phys. Discuss., 13, 17849–17900, doi:10.5194/acpd-13-17849-2013, 2013.

Gray, L. J., Beer, J., Geller, M., Haigh, J. D., Lockwood, M., Matthes, K., Cubasch, U., Fleitmann, D., Harrison, G., Hood, L., Luterbacher, J., Meehl, G. A., Shindell, D., van Geel, B., and White, W.: Solar Influences on Climate, Rev. Geophys., 48, RG4001, doi:10.1029/2009RG000282, 2010.

Huang, F. T., Mayr, H. G., Russell III, J. M., and Mlynczak, M. G.: Ozone diurnal variations in the stratosphere and lower mesosphere, based on measurements from SABER on TIMED, J. Geophys. Res., 115, D24308, doi:10.1029/2010JD014484, 2010.

Jarnot, R. F., Perun, V. S., and Schwartz, M. J.: Radiometric and spectral performance and calibration of the GHz bands of EOS MLS, IEEE T. Geosci. Remote, 44, 1131–1143, doi:10.1109/TGRS.2005.863714, 2006.

Jones, A., Urban, J., Murtagh, D. P., Eriksson, P., Brohede, S., Haley, C., Degenstein, D., Bourassa, A., von Savigny, C., Sonkaew, T., Rozanov, A., Bovensmann, H., and Burrows, J.: Evolution of stratospheric ozone and water vapour time series studied with satellite measurements, Atmos. Chem. Phys., 9, 6055–6075, doi:10.5194/acp-9-6055-2009, 2009.

Kyrölä, E., Laine, M., Sofieva, V., Tamminen, J., Päivärinta, S.-M., Tukiainen, S., Zawodny, J., and Thomason, L.: Combined SAGE II-GOMOS ozone profile data set for 1984–2011 and trend analysis of the vertical distribution of ozone, Atmos. Chem. Phys., 13, 10645–10658, doi:10.5194/acp-13-10645-2013, 2013.

Llewellyn, E. J., Lloyd, N. D., Degenstein, D. A., Gattinger, R. L., Petelina, S. V., Bourassa, A. E., Wiensz, J. T., Ivanov, E. V., McDade, I. C., Solheim, B. H., McConnell, J. C., Haley, C. S., von Savigny, C., Sioris, C. E., McLinden, C. A., Griffioen, E., Kaminski, J., Evans, W. F. J., Puckrin, E., Strong, K., Wehrle, V., Hum, R. H., Kendall, D. J. W., Matsushita, J., Murtagh, D. P., Brohede, S., Stegman, J., Witt, G., Barnes, G., Payne, W. F., Piché, L., Smith, K., Warshaw, G., Deslauniers, D.-L., Marchand, P., Richardson, E. H., King, R. A., Wevers, I., McCreath, W., Kyrölä, E., Oikarinen, L., Leppelmeier, G. W., Auvinen, H., Mégie, G., Hauchecorne, A., Lefèvre, F., de La Nöe, J., Ricaud, P., Frisk, U., Sjoberg, F., von Schéele, F., and Nordh, L.: The OSIRIS instrument on the Odin spacecraft, Can. J. Phys., 82, 411–422, 2004.

McLinden, C. A. and Fioletov, V.: Quantifying stratospheric ozone trends: Complications due to stratospheric cooling, Geophys. Res. Lett., 38, L03808, doi:10.1029/2010GL046012, 2011.

Mieruch, S., Weber, M., von Savigny, C., Rozanov, A., Bovensmann, H., Burrows, J. P., Bernath, P. F., Boone, C. D., Froidevaux, L., Gordley, L. L., Mlynczak, M. G., Russell III, J. M., Thomason, L. W., Walker, K. A., and Zawodny, J. M.: Global and long-term comparison of SCIAMACHY limb ozone profiles with correlative satellite data (2002–2008), Atmos. Meas. Tech., 5, 771–788, doi:10.5194/amt-5-771-2012, 2012.

Naujokat, B.: An update of the observed Quasi-Biennial Oscillation of stratospheric winds over the tropics, J. Atmos. Sci., 43, 1873–1877, 1986.

Nevison, C. D., Solomon, S., and Gao, R. S.: Buffering interactions in the modeled response of stratospheric O_3 to increased NO_X and HO_X, J. Geophys. Res., 104, 3741–3754, doi:10.1029/1998JD100018, 1999.

Newchurch, M. J., Yang, E.-S., Cunnold, D. M., Reinsel, G. C., Zawodny, J. M., and Russell III, J. M.: Evidence for slowdown in stratospheric ozone loss: First stage of ozone recovery, J. Geophys. Res., 108, 4507, doi:10.1029/2003JD003471, 2003.

Oman, L. D., Douglass, A. R., Ziemke, J. R., Rodriguez, J. M., Waugh, D. W., and Nielsen, J. E.: The ozone response to ENSO in Aura satellite measurements and a chemistry-climate simulation, J. Geophys. Res., 118, 965–976, doi:10.1029/2012JD018546, 2013.

Perliski, L. M., Solomon, S., and London, J.: On the interpretation of seasonal variations of stratospheric ozone, Planet. Space Sci., 37, 1527–1538, 1989.

Randel, W. J. and Thompson, A. M.: Interannual variability and trends in tropical ozone derived from SAGE II satellite data and SHADOZ ozonesondes, J. Geophys. Res., 116, D07303, doi:10.1029/2010JD015195, 2011.

Randel, W. J., Park, M., Wu, F., and Livesey, N: A large annual cycle in ozone above the tropical tropopause linked to the Brewer-Dobson circulation, J. Atmos. Sci., 64, 4479–4488, 2007.

Randel, W. J., Garcia, R. R., Calvo, N., and Marsh, D.: ENSO influence on zonal mean temperature and ozone in the tropical lower stratosphere, Geophys. Res. Lett., 36, L15822, doi:10.1029/2009GL039343, 2009.

Reinsel, G. C.: Trend analysis of upper stratospheric Umkehr ozone data for evidence of turnaround, Geophys. Res. Lett., 29, 1451, doi:10.1029/2002GL014716, 2002.

Remsberg, E. and Lingenfelser, G.: Analysis of SAGE II ozone of the middle and upper stratosphere for its response to a decadal-scale forcing, Atmos. Chem. Phys., 10, 11779–11790, doi:10.5194/acp-10-11779-2010, 2010.

Snow, M., Weber, M., Machol, J., Viereck, R., and Richard, E.: Comparison of Magnesium II core-to-wing ratio observations during solar minimum 23/24, J. Space Weather Space Clim., 4, A04, doi:10.1051/swsc/2014001, 2014.

Soukharev, B. E. and Hood, L. L.: Solar cycle variation of stratospheric ozone: Multiple regression analysis of long-term satellite data sets and comparisons with models, J. Geophys. Res., 111, D20314, doi:10.1029/2006JD007107, 2006.

SPARC CCMVal: SPARC Report on the Evaluation of Chemistry-Climate Models, Eyring, V., Shepherd, T. G., Waugh, D. W. (Eds.), SPARC Report No. 5, WCRP-132, WMO/TD-No. 1526, http://www.atmosp.physics.utoronto.ca/SPARC, 2010.

Steinbrecht, W., Claude, H., Schönenborn, F., McDermid, I. S., Leblanc, T., Godin, S., Song, T., Swart, D. P. J., Meijer, Y. J., Bodeker, G. E., Connor, B. J., Kämpfer, N., Hocke, K., Calisesi, Y., Schneider, N., de la Noë, J., Parrish, A. D., Boyd, I. S., Brühl, C., Steil, B., Giorgetta, M. A., Manzini, E., Thomason, L. W., Zawodny, J. M., McCormick, M. P., Russel III, J. M., Bhartia, P. K., Stolarski, R. S., and Hollandsworth-Frith, S. M.: Long-term evolution of upper stratospheric ozone at selected stations of the Network for the Detection of Stratospheric Change (NDSC), J. Geophys. Res., 111, D10308, doi:10.1029/2005JD006454, 2006.

Steinbrecht, W., Claude, H., Schönenborn, F., McDermid, I. S., Leblanc, T., Godin-Beekmann, S., Keckhut, P., Hauchecorne, A., Van Gijsel, J. A. E., Swart, D. P. J., Bodeker, G. E., Parrish, A., Boyd, I. S., Kämpfer, N., Hocke, K., Stolarski, R. S., Frith. S. M., Thomason, L. W., Remsberg, E. E., v. Savigny, C., Rozanov, A., and Burrows, J. P.: Ozone and temperature trends in the upper stratosphere at five stations of the Network for the Detection of Atmospheric Composition Change, Int. J. Remote Sens. , 30, 3875–2886, 2009.

Stiller, G. P., von Clarmann, T., Haenel, F., Funke, B., Glatthor, N., Grabowski, U., Kellmann, S., Kiefer, M., Linden, A., Lossow, S., and López-Puertas, M.: Observed temporal evolution of global mean age of stratospheric air for the 2002 to 2010 period, Atmos. Chem. Phys., 12, 3311–3331, doi:10.5194/acp-12-3311-2012, 2012.

Tegtmeier, S., Hegglin, M. I., Anderson, J., Bourassa, A., Brohede, S., Degenstein, D., Froidevaux, L., Fuller, R., Funke, B., Gille, J., Jones, A., Kasai, Y., Krüger, K., Kyrölä, E., Lingenfelser, G., Lumpe, J., Nardi, B., Neu, J., Pendlebury, D., Remsberg, E., Rozanov, A., Smith, L., Toohey, M., Urban, J., von Clarmann, T., Walker, K. A., and Wang, R. H. J.: SPARC Data Initiative: A comparison of ozone climatologies from international satellite limb sounders, J. Geophys. Res. Atmos., 118, 12229–12247, doi:10.1002/2013JD019877, 2013.

Thompson, A. M., Witte, J. C., McPeters, R. D., Oltmans, S. J., Schmidlin, F. J., Logan, J. A., Fujiwara, M., Kirchhoff, V. W., J. H., Posny, F., Coetzee, G. J. R., Hoegger, B., Kawakami, S., Ogawa, T., Johnson, B. J., Vömel, H., and Labow, G.: Southern Hemisphere Additional Ozonesondes (SHADOZ) 1998–2000 tropical ozone climatology 1. Comparison with Total Ozone Mapping Spectrometer (TOMS) and ground-based measurements, J. Geophys. Res., 108, 8238, doi:10.1029/2001JD000967, 2003.

Tiao, G. C., Reinsel, G. C., Xu, D., Pedrick, J. H., Zhu, X., Miller, A. J., DeLuisi, J. J., Mateer, C. L., and Wuebbles, D. J.: Effects of

autocorrelation and temporal sampling schemes on estimates of trend and spatial correlation, J. Geophys. Res., 95, 20507–20517, doi:10.1029/JD095iD12p20507, 1990.

von Savigny, C., Kaiser, J. W., Bovensmann, H., Burrows, J. P., McDermid, I. S., and Leblanc, T.: Spatial and temporal characterization of SCIAMACHY limb pointing errors during the first three years of the mission, Atmos. Chem. Phys., 5, 2593–2602, doi:10.5194/acp-5-2593-2005, 2005.

Weber, M., Dikty, S., Burrows, J. P., Garny, H., Dameris, M., Kubin, A., Abalichin, J., and Langematz, U.: The Brewer-Dobson circulation and total ozone from seasonal to decadal time scales, Atmos. Chem. Phys., 11, 11221–11235, doi:10.5194/acp-11-11221-2011, 2011.

Weber, M., Pagaran, J., Dikty, S., von Savigny, C., Burrows, J. P, DeLand, M., Floyd, L. E., Harder, J. W., Mlynczak, M. G., and Schmidt, H.: Investigation of solar irradiance variations and their impact on middle atmospheric ozone, Chapter 3, in: Climate And Weather of the Sun-Earth System (CAWSES): Highlights from a priority program, edited by: Lübken, F.-J., Springer, Dordrecht, the Netherlands, 2013.

World Meteorological Organization, Scientific Assessment of Ozone Depletion: 1998, WMO Global Ozone Research and Monitoring Project – Report No. 44, 1999.

World Meteorological Organization, Scientific Assessment of Ozone Depletion: 2006, WMO Global Ozone Research and Monitoring Project – Report No. 50, 2007.

World Meteorological Organization, Scientific Assessment of Ozone Depletion: 2010, WMO Global Ozone Research and Monitoring Project – Report No. 52, 2011.

Yang, E.-S., Cunnold, D. M., Salawitch, R. J., McCormick, M. P., Russell III, J. M., Zawodny, J. M., Oltmans, S., and Newchurch, M. J.: Attribution of recovery in lower-stratospheric ozone, J. Geophys. Res., 111, D17309, doi:10.1029/2005JD006371, 2006.

Zawodny, J. M. and McCormick, M. P.:, Stratospheric Aerosol and Gas Experiment II measurements of the quasi-biennial oscillations in ozone and nitrogen dioxide, J. Geophys. Res., 96, 9371–9377, doi:10.1029/91JD00517, 1991.